



PUBLISHED FOR SISSA BY SPRINGER

RECEIVED: April 12, 2016

REVISED: August 11, 2016

ACCEPTED: August 27, 2016

PUBLISHED: September 5, 2016

Physics reach of DUNE with a light sterile neutrino

Sanjib Kumar Agarwalla,^a Sabya Sachi Chatterjee^a and Antonio Palazzo^{b,c}

^a*Institute of Physics, Sachivalaya Marg, Sainik School Post,
Bhubaneswar 751005, India*

^b*Dipartimento Interateneo di Fisica “Michelangelo Merlin”,
Via Amendola 173, 70126 Bari, Italy*

^c*Istituto Nazionale di Fisica Nucleare (INFN), Sezione di Bari,
Via E. Orabona 4, 70126 Bari, Italy*

E-mail: sanjib@iopb.res.in, sabya@iopb.res.in, palazzo@ba.infn.it

ABSTRACT: We investigate the implications of one light eV scale sterile neutrino on the physics potential of the proposed long-baseline experiment DUNE. If the future short-baseline experiments confirm the existence of sterile neutrinos, then it can affect the mass hierarchy (MH) and CP-violation (CPV) searches at DUNE. The MH sensitivity still remains above 5σ if the three new mixing angles $(\theta_{14}, \theta_{24}, \theta_{34})$ are all close to θ_{13} . In contrast, it can decrease to 4σ if the least constrained mixing angle θ_{34} is close to its upper limit $\sim 30^\circ$. We also assess the sensitivity to the CPV induced both by the standard CP-phase $\delta_{13} \equiv \delta$, and the new CP-phases δ_{14} and δ_{34} . In the 3+1 scheme, the discovery potential of CPV induced by δ_{13} gets deteriorated compared to the 3ν case. In particular, the maximal sensitivity (reached around $\delta_{13} \sim \pm 90^\circ$) decreases from 5σ to 4σ if all the three new mixing angles are close to θ_{13} . It can further diminish to almost 3σ if θ_{34} is large ($\sim 30^\circ$). The sensitivity to the CPV due to δ_{14} can reach 3σ for an appreciable fraction of its true values. Interestingly, θ_{34} and its associated phase δ_{34} can influence both the ν_e appearance and ν_μ disappearance channels via matter effects, which in DUNE are pronounced. Hence, DUNE can also probe CPV induced by δ_{34} provided θ_{34} is large. We also reconstruct the two phases δ_{13} and δ_{14} . The typical 1σ uncertainty on δ_{13} (δ_{14}) is $\sim 20^\circ$ (30°) if $\theta_{34} = 0$. The reconstruction of δ_{14} (but not that of δ_{13}) degrades if θ_{34} is large.

KEYWORDS: Neutrino Physics, Beyond Standard Model

ARXIV EPRINT: [1603.03759](https://arxiv.org/abs/1603.03759)

Contents

1	Introduction and motivation	1
2	Transition probability in the 3+1 scheme	3
2.1	Theoretical framework	3
2.2	Transition probability in Vacuum	4
2.3	Transition probability in matter	4
3	Description of DUNE setup and statistical analysis	8
4	Mass hierarchy discovery potential in the 3+1 scheme	10
4.1	Discussion at the level of bi-events plots	11
4.2	Role of the energy spectrum	12
4.3	Numerical results	13
5	CP-violation searches in the 3+1 scheme	14
5.1	CP-violation discovery potential	14
5.2	Reconstruction of the CP-phases	17
6	Conclusions and outlook	20

1 Introduction and motivation

The high energy physics community is devoting enormous effort at the cosmic, intensity, and energy frontiers to unravel the deep long-standing mysteries of the Universe. At the forefront of the intensity frontier, ambitious next-generation, long-baseline (LBL) neutrino oscillation experiments are under consideration [1–5], whose mission will be that of deciphering the fundamental properties of these elusive particles, and of the interactions to which they participate. The main objectives of the LBL experiments are to determine the leptonic CP-violation (CPV), and to identify the neutrino mass hierarchy (MH). However, the actual scope of these projects is much broader and to some extent unknown. As a matter of fact, these setups are potentially able to unveil physics beyond the Standard Model, which may be disguised in the form of new neutrino interactions or states.

The LBL experiments are high-precision neutrino interferometers, and as such, they are the best place to study CPV, whose manifestation is intimately related to interference phenomena. This is clearly the case of the standard 3-flavor CPV, which is observable through the interference of the oscillations driven by the two distinct (atmospheric and solar) frequencies. Several non-standard neutrino properties are sources of additional CPV,

and the LBL machines would naturally have a pivotal role also in these searches. Interestingly, as first evidenced in [6], the LBL experiments may be sensitive to the new CP-phases arising in the presence of a light sterile neutrino state.

Sterile neutrinos represent one of the simplest and most “innocuous” extensions of the Standard Model and naturally appear in many mechanisms of generation of the neutrino masses. Intriguingly, a series of anomalies recorded at the short baseline experiments, lends support to the existence of such new neutrino states (see [7–9] for a review of the topic). These phenomena cannot be accommodated in the 3-flavor framework, and require the existence of a fourth mostly sterile mass eigenstate at the scale of ~ 1 eV.

A rich and diverse program of new short-baseline (SBL) experiments is underway to test such a hypothesis (see the review in [10]). The SBL experiments are surely the best place where to look for light sterile neutrinos. In fact, at the short baselines, the characteristic oscillating behavior driven by the new mass-squared splitting $\Delta m_{\text{new}}^2 \sim 1 \text{ eV}^2$ should show up. On the other hand, the SBL experiments cannot probe all the properties of sterile neutrinos. In particular, they are not sensitive to the new CPV¹ phenomena implied by the sterile neutrinos, which need long distances to develop at a detectable level. Therefore, in the eventuality of a discovery of a light sterile neutrino, the LBL setups would play a complementary role to the SBL experiments, due to their unique sensitivity to the new CP-phases.

An unavoidable (less desired) byproduct of this circumstance is that the performance of the LBL machines towards their original targets tends to be deteriorated in the presence of sterile neutrinos. This is evident for the CPV, since the new CP-phases tend to be degenerate with the standard CP-phase δ . In addition, the well-known degeneracy between MH and CPV, already existing in the 3-flavor scheme, is exacerbated in the presence of the new CP-phases. Consequently, the MH discovery potential can also be reduced. Therefore, in view of the potential discovery of a light eV-scale sterile neutrino at the SBL experiments, a reassessment of the performance of the planned LBL projects appears to be mandatory.

The 4-flavor analyses² [6, 13] of the latest data collected by the two currently running LBL experiments T2K and NO ν A³ have given already some weak hints on the new CP-phases involved in the 3+1 scheme, and have also evidenced the fragility of the present (weak) indication in favor of the normal hierarchy, which emerges in the standard 3-flavor framework. In addition, in the recent prospective study [18] of T2K and NO ν A, it has been pointed out that even considering the full exposure regime for such two experiments, their

¹In the 3+1 scheme with one light eV-scale sterile neutrino, the oscillation picture at the SBL experiments essentially boils down to the 2-flavor scheme, and therefore, one cannot observe CPV. When more sterile neutrinos come into play the SBL experiments can be sensitive to CPV. However, the SBL experiments can access only a restricted number of the CP-phases involved in the model, while the LBL ones are sensitive to all of them. For example, in the 3+2 scheme, the SBL experiments are sensitive to one CP-phase over a total of five CP-phases.

²Such analyses are performed for realistic values of the new active-sterile mixing angles as indicated by the global 3+1 fits [11, 12].

³In principle (see the 4-flavor analysis performed in [14]), the new CP-phases can impact also the $\nu_\mu \rightarrow \nu_e$ searches of ICARUS [15, 16] and OPERA [17]. However, the very low statistics prevents to extract any information on the CP-phases.

sensitivity to the standard CP-phase δ , and their discovery potential of the neutrino mass hierarchy both get deteriorated in the presence of a sterile neutrino. Therefore, the next natural step is to investigate the impact of a sterile neutrino at the more sensitive next-generation LBL facilities. In the present work, we focus on the proposed Deep Underground Neutrino Experiment (DUNE), which is aiming to achieve new heights in the intensity frontier by shooting a very powerful neutrino beam from Fermilab towards the Homestake Mine in South Dakota over a distance of 1300 km.⁴ Our work complements other recent studies performed about DUNE [23–25]. Previous studies on sterile neutrinos at LBL experiments can be found in [26–34].

The paper is organized as follows. In section 2, we introduce the theoretical framework and present a detailed discussion of the behavior of the 4-flavor $\nu_\mu \rightarrow \nu_e$ transition probabilities in vacuum and in matter. In section 3, we describe the details of the DUNE setup and of the statistical analysis. In section 4, we make some important considerations at the level of the bi-events plots and at the level of the energy spectrum, and then we present the results of the sensitivity study of the mass hierarchy in the 3+1 scheme. Section 5 is devoted to the results concerning the CPV discovery potential and the capability of reconstruction of the CP-phases. Finally, we draw our conclusions in section 6.

2 Transition probability in the 3+1 scheme

2.1 Theoretical framework

In the 3+1 scheme, there is one sterile neutrino ν_s and the flavor basis is connected to the mass one through a 4×4 matrix, which can be conveniently parametrized as follows

$$U = \tilde{R}_{34} R_{24} \tilde{R}_{14} R_{23} \tilde{R}_{13} R_{12}, \quad (2.1)$$

where R_{ij} (\tilde{R}_{ij}) is a real (complex) 4×4 rotation in the (i, j) plane containing the 2×2 matrix

$$R_{ij}^{2 \times 2} = \begin{pmatrix} c_{ij} & s_{ij} \\ -s_{ij} & c_{ij} \end{pmatrix} \quad \tilde{R}_{ij}^{2 \times 2} = \begin{pmatrix} c_{ij} & \tilde{s}_{ij} \\ -\tilde{s}_{ij}^* & c_{ij} \end{pmatrix}, \quad (2.2)$$

in the (i, j) sub-block, where we have defined

$$c_{ij} \equiv \cos \theta_{ij} \quad s_{ij} \equiv \sin \theta_{ij} \quad \tilde{s}_{ij} \equiv s_{ij} e^{-i\delta_{ij}}. \quad (2.3)$$

The parameterization in eq. (2.1) enjoys the following properties: i) When the mixing involving the fourth state is zero ($\theta_{14} = \theta_{24} = \theta_{34} = 0$) it returns the 3ν matrix in its common parameterization. ii) For small values of θ_{13} and of the mixing angles involving ν_4 , one has $|U_{e3}|^2 \simeq s_{13}^2$, $|U_{e4}|^2 = s_{14}^2$, $|U_{\mu 4}|^2 \simeq s_{24}^2$ and $|U_{\tau 4}|^2 \simeq s_{34}^2$, with a clear physical interpretation of the new mixing angles. iii) The leftmost positioning of the matrix \tilde{R}_{34} guarantees that the vacuum $\nu_\mu \rightarrow \nu_e$ transition probability is independent of θ_{34} and of the related CP-phase δ_{34} (see [6]).

⁴The CERN-Pyhäsalmi baseline of 2290 km actively studied under the umbrella of the LBNO collaboration [19, 20] can also be very sensitive to these issues. The same is also true for the future T2HK experiment [21, 22], which is a bigger version of T2K.

2.2 Transition probability in Vacuum

In the DUNE setup the matter effects play an important role. However, for the sake of clearness, before discussing the flavor conversion in the presence of matter we give a brief sketch of the basic formulae in vacuum. This will help the reader to grasp some new qualitative features, which emerge solely in the presence of matter. As shown in [6], the $\nu_\mu \rightarrow \nu_e$ conversion probability can be written as the sum of three contributions

$$P_{\mu e}^{4\nu} \simeq P^{\text{ATM}} + P_{\text{I}}^{\text{INT}} + P_{\text{II}}^{\text{INT}}. \quad (2.4)$$

The first term is positive-definite and is related to the atmospheric mass-squared splitting. It gives the leading contribution to the probability and can be written as

$$P^{\text{ATM}} \simeq 4s_{23}^2 s_{13}^2 \sin^2 \Delta, \quad (2.5)$$

where $\Delta \equiv \Delta m_{31}^2 L/4E$ is the atmospheric oscillating factor, which depends on the baseline L and the neutrino energy E . The second and third contributions in eq. (2.4) are interference terms and, as such, they can assume both positive and negative values. The second term is driven by the standard solar-atmospheric interference and can be approximately expressed as

$$P_{\text{I}}^{\text{INT}} \simeq 8s_{13}s_{12}c_{12}s_{23}c_{23}(\alpha\Delta) \sin \Delta \cos(\Delta + \delta_{13}). \quad (2.6)$$

The third term is related to the atmospheric-sterile interference and has the following form [6]

$$P_{\text{II}}^{\text{INT}} \simeq 4s_{14}s_{24}s_{13}s_{23} \sin \Delta \sin(\Delta + \delta_{13} - \delta_{14}). \quad (2.7)$$

The transition probability depends on the three small mixing angles θ_{13} , θ_{14} , θ_{24} , whose best estimates, derived from the global 3-flavor analyses [35–37] (concerning θ_{13}) and from the 3+1 fits [11, 12] (concerning θ_{14} and θ_{24}), turn out to be very similar and we have approximately $s_{13} \sim s_{14} \sim s_{24} \sim 0.15$ (see table 1). Therefore, it is meaningful to treat all such three mixing angles as small quantities of the same order ϵ . Another small quantity entering the transition probability is the ratio of the solar over the atmospheric mass-squared splitting $\alpha \equiv \Delta m_{21}^2/\Delta m_{31}^2 \simeq \pm 0.03$, which can be assumed to be of order ϵ^2 . From eqs. (2.5)–(2.7) we see that the first leading term is of the second order, while the two interference terms are both of the third order. Hence, the amplitudes of the two interference terms can be similar.

Before closing this subsection, we would like to highlight the fact that the transition probability in vacuum does not depend on the third mixing angle θ_{34} and on the associated CP-phase δ_{34} . As we will discuss in the next subsection, this is no more true in the presence of matter, where such a dependency emerges.

2.3 Transition probability in matter

In the presence of matter, the Hamiltonian in the flavor basis can be written as

$$H = UKU^\dagger + V, \quad (2.8)$$

where K denotes the diagonal matrix containing the wave numbers

$$K = \text{diag}(0, k_{21}, k_{31}, k_{41}), \quad (2.9)$$

with $k_{i1} = \Delta m_{i1}^2/2E$ ($i = 2, 3, 4$) and V is the matrix encoding the matter potential

$$V = \text{diag}(V_{CC}, 0, 0, -V_{NC}), \quad (2.10)$$

where

$$V_{CC} = \sqrt{2} G_F N_e \quad (2.11)$$

is the charged-current interaction potential of the electron neutrinos with the background electrons having number density N_e , and

$$V_{NC} = -\frac{1}{2} \sqrt{2} G_F N_n \quad (2.12)$$

is the neutral-current interaction potential (common to all the active neutrino species) with the background neutrons having number density N_n . For later convenience, we also introduce the positive-definite ratio

$$r = -\frac{V_{NC}}{V_{CC}} = \frac{1}{2} \frac{N_n}{N_e}, \quad (2.13)$$

which in the Earth crust is $r \simeq 0.5$. In order to simplify the treatment of matter effects, it is useful to introduce the new basis

$$\bar{\nu} = \bar{U}^\dagger \nu, \quad (2.14)$$

where

$$\bar{U} = \tilde{R}_{34} R_{24} \tilde{R}_{14} \quad (2.15)$$

is the part of the mixing matrix defined in eq. (2.1) that contains only the rotations involving the fourth neutrino mass eigenstate. The mixing matrix U is split as follows

$$U = \bar{U} U_{3\nu} \quad (2.16)$$

where $U_{3\nu}$ is the 4×4 matrix which contains the standard 3-flavor mixing matrix in the (1,2,3) sub-block. In the new basis, the Hamiltonian takes the form

$$\bar{H} = \bar{H}^{\text{kin}} + \bar{H}^{\text{dyn}} = U_{3\nu} K U_{3\nu}^\dagger + \bar{U}^\dagger V \bar{U}, \quad (2.17)$$

where the first term is the kinematic contribution describing the oscillations in vacuum, and the second one represents a nonstandard dynamical term. As shown in [6] (see the appendix), since $|k_{41}|$ is much bigger than one and much bigger than $|k_{21}|$ and $|k_{31}|$, one can reduce the dynamics to an effective 3-flavor system. Indeed, from eq. (2.17) one has that the (4,4) entry of \bar{H} is much bigger than all the other elements and the fourth eigenvalue of \bar{H} is much larger than the other three ones. As a result, the state $\bar{\nu}_s$ evolves independently of the others. Extracting the submatrix with indices (1, 2, 3) from \bar{H} , one obtains the 3×3 Hamiltonian

$$\bar{H}_{3\nu} = \bar{H}_{3\nu}^{\text{kin}} + \bar{H}_{3\nu}^{\text{dyn}} \quad (2.18)$$

governing the evolution of the $(\bar{\nu}_e, \bar{\nu}_\mu, \bar{\nu}_\tau)$ system, whose dynamical part has the form [6]

$$\bar{H}_{3\nu}^{\text{dyn}} = V_{CC} \begin{bmatrix} |\bar{U}_{e1}|^2 + r|\bar{U}_{s1}|^2 & r\bar{U}_{s1}^* \bar{U}_{s2} & r\bar{U}_{s1}^* \bar{U}_{s3} \\ \dagger & r|\bar{U}_{s2}|^2 & r\bar{U}_{s2}^* \bar{U}_{s3} \\ \dagger & \dagger & r|\bar{U}_{s3}|^2 \end{bmatrix}, \quad (2.19)$$

where we have indicated with \dagger the complex conjugate of the element with the same two indices inverted. In deriving eq. (2.19) we have used the relations $\bar{U}_{e2} = \bar{U}_{e3} = \bar{U}_{\mu 3} = 0$. Considering the explicit expressions of the elements of \bar{U} , and taking their first-order expansion in the small mixing angles θ_{i4} ($i = 1, 2, 3$), eq. (2.19) takes the form

$$\bar{H}_{3\nu}^{\text{dyn}} \approx V_{CC} \begin{bmatrix} 1 - (1-r)s_{14}^2 & r\tilde{s}_{14}s_{24} & r\tilde{s}_{14}\tilde{s}_{34}^* \\ \dagger & rs_{24}^2 & rs_{24}\tilde{s}_{34}^* \\ \dagger & \dagger & rs_{34}^2 \end{bmatrix}. \quad (2.20)$$

From eq. (2.20) we see that for vanishing sterile neutrino angles ($\theta_{14} = \theta_{24} = \theta_{34} = 0$) one recovers the (diagonal) standard 3-flavor MSW Hamiltonian. In general, in the 4-flavor case, the Hamiltonian in eq. (2.20) encodes both diagonal and off-diagonal perturbations. We can observe that these corrections are formally equivalent to non-standard neutrino interactions (NSI)⁵

$$\bar{H}_{3\nu}^{\text{dyn}} \approx V_{CC} \begin{bmatrix} 1 + \varepsilon_{ee} & \varepsilon_{e\mu} & \varepsilon_{e\tau} \\ \dagger & \varepsilon_{\mu\mu} & \varepsilon_{\mu\tau} \\ \dagger & \dagger & \varepsilon_{\tau\tau} \end{bmatrix}. \quad (2.21)$$

This formal analogy is helpful to qualitatively understand the sensitivity to the new dynamical effects implied by the sterile neutrinos. It is well known that in the $\nu_\mu \rightarrow \nu_e$ channel, the NSI that play the most important role are $\varepsilon_{e\mu}$ and $\varepsilon_{e\tau}$, while in the $\nu_\mu \rightarrow \nu_\mu$ channel $\varepsilon_{\mu\tau}$ has the biggest impact. If one assumes that the three new mixing angles have the same value $s_{14}^2 = s_{24}^2 = s_{34}^2 = 0.025$, all the corrections in eq. (2.21) are very small ($|\varepsilon_{\alpha\beta}| \simeq 0.01$) and they have a negligible impact. In this case, the dynamics is almost equivalent to that of the standard 3-flavor case. In contrast, if one allows the third mixing angle to assume values close to its upper bound ($\theta_{34} \sim 30^\circ$), the elements of the third column of the Hamiltonian in eq. (2.21) can be appreciably larger ($|\varepsilon_{e\tau}| \simeq |\varepsilon_{\mu\tau}| \simeq 0.04$ and $|\varepsilon_{\tau\tau}| \simeq 0.13$). In this last case, one may expect a noticeable impact of $\varepsilon_{e\tau} \equiv r\tilde{s}_{14}\tilde{s}_{34}^*$ in the $\nu_\mu \rightarrow \nu_e$ appearance probability, and of $\varepsilon_{\mu\tau} \equiv rs_{24}\tilde{s}_{34}^*$ in the $\nu_\mu \rightarrow \nu_\mu$ survival probability. As a consequence both channels should have some sensitivity to the third CP-phase δ_{34} since $\tilde{s}_{34}^* \equiv s_{34}e^{i\delta_{34}}$. Therefore, in contrast to the vacuum case, in matter, the flavor conversion is sensitive to the two parameters θ_{34} and δ_{34} . Concerning the $\nu_\mu \rightarrow \nu_e$ appearance probability, this behavior has been already pointed out in the analytical treatment presented in [6] (see the

⁵We stress that this is only a formal analogy. The real NSI are mediated by heavy particles. In contrast, in the case of sterile neutrinos there is no heavy mediator and the NSI-like structure of the Hamiltonian is merely related to the fact that we are working in the new basis introduced in eq. (2.14), which is rotated with respect to the original flavor basis and is particularly convenient to handle the problem under consideration. It is worthwhile to mention that a similar analogy has been noticed concerning the solar neutrino transitions in the presence of sterile species [38].

appendix therein), and successively noticed in the numerical simulations performed in [25]. Regarding the $\nu_\mu \rightarrow \nu_\mu$ survival probability, to our knowledge the dependency on $(\theta_{34}, \delta_{34})$ has not been noted before in the literature. The dependency of both channels from these parameters represents a very interesting feature, because in favorable circumstances (i.e., a large value of θ_{34}), the LBL experiments may be sensitive not only to the two CP-phases δ_{13} and δ_{14} but also to the CP-phase δ_{34} . Hence, the searches performed at DUNE may provide full access to the rich CPV structure of the 3+1 scheme. In order to illustrate the peculiar role of the third mixing angle, in our numerical study we will consider the following three benchmark cases: $\theta_{34} = 0$, $\theta_{34} = 9^\circ$ (i.e., equal to the other two mixing angles θ_{14} and θ_{24}) and $\theta_{34} = 30^\circ$ (which is a value close to its current upper bound). For clarity, we report these values in the second column of table 1.

For completeness, we show how to proceed to calculate the oscillation probabilities in matter, by reducing the dynamics of the 4-flavor system to that of a 3-flavor one [6]. To this purpose, it is helpful to define the evolution operator, which, in the rotated basis $\bar{\nu}$, has the form

$$\bar{S} \equiv e^{-i\bar{H}L} \approx \begin{pmatrix} e^{-i\bar{H}_{3\nu}L} & \mathbf{0} \\ \mathbf{0} & e^{-ik_{41}L} \end{pmatrix}, \quad (2.22)$$

and is related to the evolution operator in the original flavor basis by the unitary transformation

$$S = \bar{U}\bar{S}\bar{U}^\dagger. \quad (2.23)$$

The S matrix describes the flavor conversion after traversing the distance L

$$\nu_\beta(L) = S_{\beta\alpha}\nu_\alpha(0), \quad (2.24)$$

and the 4-flavor oscillation probability is given by⁶

$$P_{\alpha\beta}^{4\nu} \equiv P^{4\nu}(\nu_\alpha \rightarrow \nu_\beta; L) = |S_{\beta\alpha}|^2. \quad (2.25)$$

The block-diagonal form of \bar{S} allows us to express the elements of S in terms of those of \bar{S} and thus reduce the 4-flavor problem to a 3-flavor one. In fact, exploiting the relations $\bar{U}_{e2} = \bar{U}_{e3} = \bar{U}_{\mu3} = 0$, one can easily derive the following expression for the $\nu_\mu \rightarrow \nu_e$ transition amplitude and for that of the $\nu_\mu \rightarrow \nu_\mu$ survival amplitude

$$S_{e\mu} = \bar{U}_{e1} [\bar{U}_{\mu1}^* \bar{S}_{ee} + \bar{U}_{\mu2}^* \bar{S}_{e\mu}] + \bar{U}_{e4} \bar{U}_{\mu4}^* \bar{S}_{ss}, \quad (2.26)$$

$$S_{\mu\mu} = \bar{U}_{\mu1}^* [\bar{U}_{\mu1} \bar{S}_{ee} + \bar{U}_{\mu2} \bar{S}_{e\mu}] + \bar{U}_{\mu2}^* [\bar{U}_{\mu1} \bar{S}_{e\mu} + \bar{U}_{\mu2} \bar{S}_{\mu\mu}] + |\bar{U}_{\mu4}|^2 \bar{S}_{ss}, \quad (2.27)$$

where the five relevant matrix elements of the matrix \bar{U} are given by

$$\begin{aligned} \bar{U}_{e1} &= c_{14} \\ \bar{U}_{\mu1} &= s_{14}s_{24}e^{i\delta_{14}} \\ \bar{U}_{\mu2} &= c_{24} \\ \bar{U}_{e4} &= s_{14}e^{-i\delta_{14}} \\ \bar{U}_{\mu4} &= c_{14}s_{24}. \end{aligned} \quad (2.28)$$

⁶Note the inverted order of the two flavor indexes α and β in the definitions of the oscillation probability and of the evolution operator.

We can immediately observe that in vacuum, both $S_{e\mu}$ and $S_{\mu\mu}$ are independent of the mixing angle θ_{34} and the associated CP-phase δ_{34} . In fact, in vacuum, the elements of \bar{S} exactly return the corresponding 3-flavor expressions, which may depend solely on the CP-phase δ_{13} . Therefore, in vacuum, both the ν_e appearance and ν_μ disappearance oscillation probabilities depend only on the two CP-phases δ_{13} and δ_{14} . In addition, we have verified that the ν_μ disappearance probability depends very weakly on such two phases. In contrast, in matter, $S_{e\mu}$ and $S_{\mu\mu}$ depend on the mixing angle θ_{34} and on its associated CP-phase δ_{34} through the elements \bar{S}_{ee} , $\bar{S}_{e\mu}$, $\bar{S}_{\mu e}$ and $\bar{S}_{\mu\mu}$. As discussed above, this is due to the NSI-like structure of the matter term of the Hamiltonian in the rotated basis [see eq. (2.20) and eq. (2.21)]. Taking the modulus squared of the elements $S_{e\mu}$ and $S_{\mu\mu}$ in eqs. (2.26)–(2.27) one arrives at the expressions of the ν_e appearance and ν_μ disappearance probabilities. In the calculation one should take into account that $\bar{S}_{ss} = e^{-ik_{41}L}$ oscillates very fast, and that all the associated terms are averaged by the energy resolution of the detector.

3 Description of DUNE setup and statistical analysis

Hosted at Fermilab, DUNE is a next-generation long-baseline neutrino oscillation experiment which will play an important role in the future neutrino roadmap to unravel the fundamental properties of neutrino [39–43]. DUNE is a quite ambitious project, and to accomplish its broad and rich physics objectives as a world-class facility, it is needed to develop three major components: a) an intense (\sim megawatt), wide-band neutrino beam at Fermilab, b) a fine-grained, high-precision near neutrino detector just downstream of the neutrino source, and c) a massive (\sim 40 kt) liquid argon time-projection chamber (LArTPC) far detector housed deep underground at the Sanford Underground Research Facility (SURF) 1300 km away in Lead, South Dakota. The LArTPC technology is quite effective for uniform and high accuracy imaging of massive active volumes [44]. One of the merits of a LArTPC is that it works like a totally active calorimeter where one can detect the energy deposited by all final-state particles, providing an excellent energy resolution over a wide range of energies inevitable to study the first and second oscillation maxima. We assume a fiducial mass of 35 kt for the far detector in our simulation, and consider the detector properties which are given in table 1 of ref. [19]. As far as the neutrino beam specifications are concerned, we consider a proton beam power of 708 kW in its initial phase with a proton energy of 120 GeV which can deliver 6×10^{20} protons on target in 230 days per calendar year. In our simulation, we have used the fluxes which were estimated assuming a decay pipe length of 200 m and 200 kA horn current [45]. We consider a total run time of ten years for this experiment which is equivalent to a total exposure of 248 kt \cdot MW \cdot year. We assume that the DUNE experiment would use half of its full exposure in the neutrino mode, and the remaining half would be used during antineutrino run. In our simulation, we take the reconstructed neutrino and anti-neutrino energy range to be 0.5 GeV to 10 GeV. To incorporate the systematic uncertainties, we consider an uncorrelated 5% normalization error on signal, and 5% normalization error on background for both the appearance and disappearance channels to analyze the prospective data from the DUNE experiment. We consider the same set of systematics for both the neutrino

and antineutrino channels which are also uncorrelated. For both ν_e and $\bar{\nu}_e$ appearance channels, the backgrounds mainly arise from three different sources: a) the intrinsic $\nu_e/\bar{\nu}_e$ contamination of the beam, b) the number of muon events which will be misidentified as electron events, and c) the neutral current events. Our assumptions on various components of the DUNE set-up are slightly different compared to what have been considered for the Conceptual Design Report (CDR) reference design in ref. [40].⁷ It has been shown in ref. [40] that considering the CDR reference beam design and with an exposure of 1320 kt · MW · year, CPV can be determined for 75% of δ values at 3σ confidence level. We have checked that similar coverage in δ values for establishing CPV can be achieved with our assumptions on the DUNE setup if we consider the same amount of exposure and the same oscillation parameters.

The experimental sensitivities presented in this work are estimated using the GLoBES software [46, 47] along with its new physics tools. We incorporate the 4-flavor effects both in the $\nu_\mu \rightarrow \nu_e$ appearance channel, and in the $\nu_\mu \rightarrow \nu_\mu$ disappearance channel. The same is also true for the anti-neutrino mode. We take the neutrino interaction cross-sections from refs. [48, 49], where the authors gave the cross-section for water and isoscalar targets. To obtain cross-sections for LAr, we have scaled the inclusive charged current cross-sections of water by a factor of 1.06 for neutrino, and 0.94 for anti-neutrino [50, 51]. The details of the statistical method that we follow in the present work, are exactly similar to what have been described in section 4 of ref. [18]. The only difference that we have in the present paper is that, we have also analyzed the cases where the active-sterile mixing angle θ_{34} , and its associated CP-phase δ_{34} are non-zero, since the impact of these parameters can be noticeable for the DUNE baseline as can be seen from our sensitivity results which we present in the next sections. Table 1 shows the true values of the oscillation parameters and their marginalization ranges which we consider in our simulation. As far as the mixing angles involving the fourth state are concerned (θ_{14} , θ_{24} , and θ_{34}), we take their values to be fixed as given in table 1 while generating the data and also in the fit. For non-zero $\sin^2 \theta_{34}$, we take the true values of 0.025 and 0.25 which are well within its allowed range [11, 12]. We vary the true values of δ_{14} and δ_{34} in their allowed ranges of $[-\pi, \pi]$, and they have been marginalized over their full ranges in the fit as required. We consider the mass-squared splitting $\Delta m_{41}^2 = 1 \text{ eV}^2$, which is the value currently suggested by the SBL anomalies. However, we stress that our results would be unchanged for different choices of this parameter, provided that $\Delta m_{41}^2 \gtrsim 0.1 \text{ eV}^2$. For such values, the very fast oscillations driven by the new large mass-squared splitting are completely averaged by the finite energy resolution of the detector. For the same reason, DUNE is insensitive to $\text{sgn}(\Delta m_{41}^2)$ and we can confine our study to positive values. For the 2-3 mixing angle, we consider the maximal mixing ($\pi/4$) as the true value, and in the fit, we marginalize over the range given in table 1. We marginalize over both the choices of hierarchy in the fit for all the analyses, except for the mass hierarchy discovery studies where our goal is to exclude the

⁷But, needless to mention, these assumptions on the beam fluxes, various detector characteristics, and systematic uncertainties are preliminary, and are expected to evolve with time as our understanding about the key components of the DUNE experiment is going to be refined/improved with the help of ongoing R&D efforts.

Parameter	True Value	Marginalization Range
$\sin^2 \theta_{12}$	0.304	Not marginalized
$\sin^2 2\theta_{13}$	0.085	Not marginalized
$\sin^2 \theta_{23}$	0.50	[0.34, 0.68]
$\sin^2 \theta_{14}$	0.025	Not marginalized
$\sin^2 \theta_{24}$	0.025	Not marginalized
$\sin^2 \theta_{34}$	0, 0.025, 0.25	Not marginalized
$\delta_{13}/^\circ$	$[-180, 180]$	$[-180, 180]$
$\delta_{14}/^\circ$	$[-180, 180]$	$[-180, 180]$
$\delta_{34}/^\circ$	$[-180, 180]$	$[-180, 180]$
$\frac{\Delta m_{21}^2}{10^{-5} \text{ eV}^2}$	7.50	Not marginalized
$\frac{\Delta m_{31}^2}{10^{-3} \text{ eV}^2}$ (NH)	2.475	Not marginalized
$\frac{\Delta m_{31}^2}{10^{-3} \text{ eV}^2}$ (IH)	-2.4	Not marginalized
$\frac{\Delta m_{41}^2}{\text{eV}^2}$	1.0	Not marginalized

Table 1. Parameter values/ranges used in the numerical calculations. The second column reports the true values of the oscillation parameters used to simulate the “observed” data set. The third column reports the range over which $\sin^2 \theta_{23}$, and the three CP-phases δ_{13} , δ_{14} and δ_{34} are varied while minimizing the χ^2 to obtain the final results.

wrong hierarchy in the fit. We take the line-averaged constant Earth matter density⁸ of 2.87 g/cm^3 for the DUNE baseline. In our calculation, we do not explicitly consider the near detector of DUNE which may provide some information on θ_{14} and θ_{24} , but certainly, the near detector data are not sensitive to the CP-phases in which we are interested. In our simulation, we have performed a full spectral analysis using the binned events spectra for the DUNE setup. In the numerical analysis, the Poissonian $\Delta\chi^2$ is marginalized over the uncorrelated systematic uncertainties using the method of pulls as described in refs. [53, 54]. To present the results, we display the 1, 2, 3 σ confidence levels for 1 d.o.f. using the relation $N\sigma \equiv \sqrt{\Delta\chi^2}$. In [55], it was demonstrated that the above relation is valid in the frequentist method of hypothesis testing.

4 Mass hierarchy discovery potential in the 3+1 scheme

In this section, we discuss the sensitivity of DUNE to the neutrino mass hierarchy. As a first step we provide a description at the level of the signal events aided by bi-event plots. Second, we highlight the role of the spectral shape information in the hierarchy discrimination. Finally, we present the results of the full numerical analysis.

⁸The line-averaged constant Earth matter density has been computed using the Preliminary Reference Earth Model (PREM) [52].

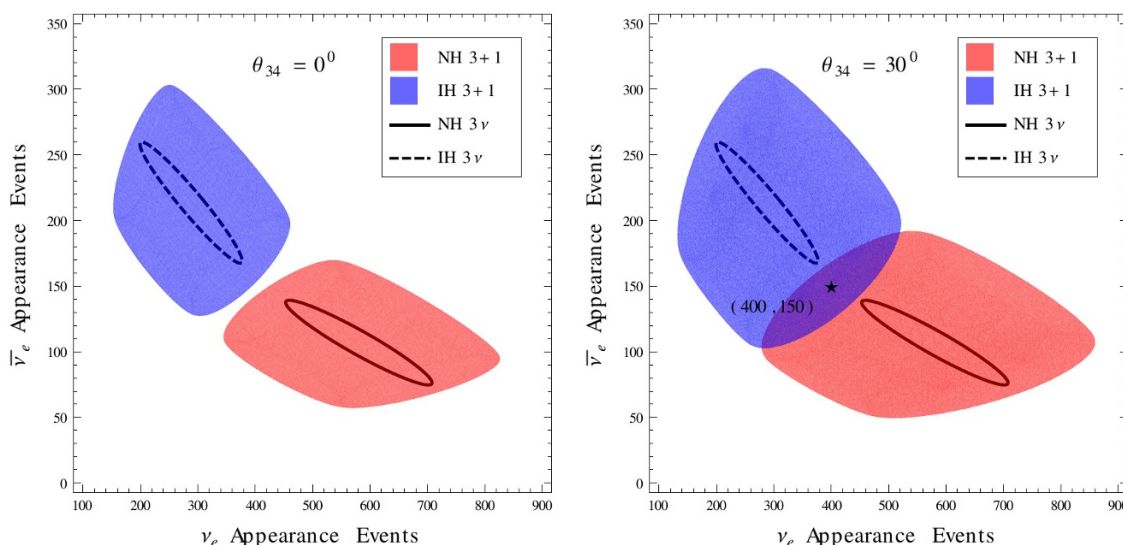


Figure 1. The colored shaded blobs represent the bi-event plots for DUNE in the 3+1 scheme. The left panel corresponds to the case $\theta_{34} = 0^\circ$, while the right panel corresponds to the case $\theta_{34} = 30^\circ$. The blobs in the left panel are obtained by varying the CP-phases δ_{13} and δ_{14} in the range $[-\pi, \pi]$. In the right panel also the CP-phase δ_{34} is allowed to vary in the same range. The black curves show the 3-flavor ellipses for comparison. In this case, there is only one running parameter, which is the CP-phase δ_{13} .

4.1 Discussion at the level of bi-events plots

In figure 1, we introduce the bi-event plots, in which the two axes represent the total number of ν_e (x -axis) and $\bar{\nu}_e$ (y -axis) events.⁹ In both panels, the 3-flavor case is represented by the black ellipses, which are obtained varying the CP-phase δ_{13} in the range $[-\pi, \pi]$. In the 3+1 scheme, there are more CP-phases and the bi-event plot becomes a blob. In particular in the left panel, where we have taken $\theta_{34} = 0$, we vary the two phases δ_{13} and δ_{14} in the range $[-\pi, \pi]$. In addition, in the right panel, which corresponds to $\theta_{34} = 30^\circ$, we also vary the phase δ_{34} in the same range. The 3+1 blobs can be seen as a convolution of an infinite ensemble of ellipses having different orientations or, alternatively, as a scatter plot obtained by varying simultaneously the CP-phases δ_{13} , δ_{14} (and also δ_{34} in the right panel). One can see that in both the panels, the separation between the blobs corresponding to the two different hierarchies in the 3+1 scheme gets reduced as compared to the 3-flavor ellipses. In particular, as evident from the right panel, for $\theta_{34} = 30^\circ$, there is a region where the two hierarchies overlap. For each point of this region, there are two possible choices of the three CP-phases (one choice corresponding to NH and the other one to IH). In these cases, there is a complete degeneracy between the two hierarchies at the level of the total number of events (both neutrino and antineutrino), and the information based on total event rates cannot distinguish between NH and IH. The point marked by star in the right

⁹In the 3+1 scheme, these kind of plots were introduced for the first time in ref. [18] in the context of T2K and NO ν A.

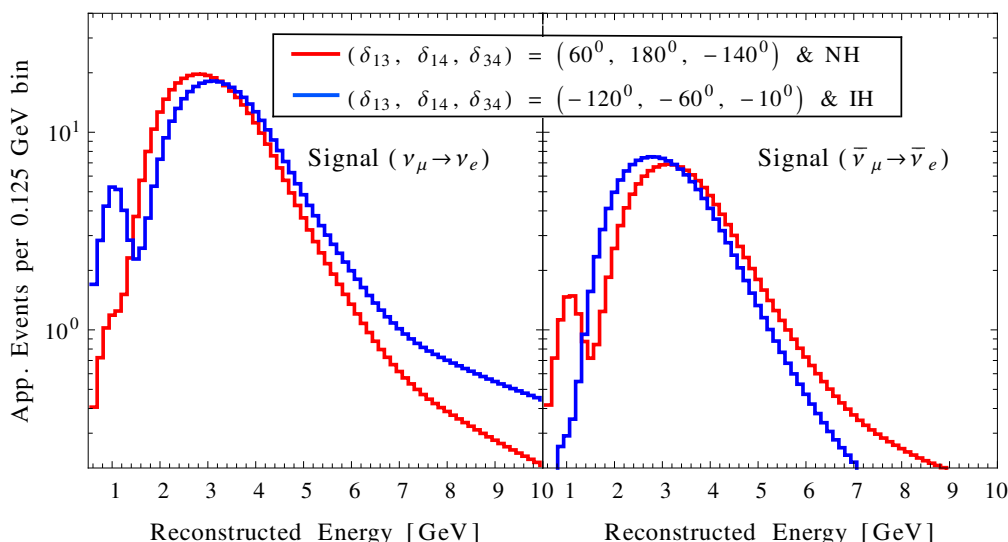


Figure 2. Expected signal event spectrum of DUNE for the ν_e (left panel) and $\bar{\nu}_e$ (right panel) appearance channel as a function of the reconstructed neutrino energy. The red (blue) histogram corresponds to the case of NH (IH). All the spectra are obtained for $\theta_{34} = 30^\circ$. For the values of the three CP-phases $(\delta_{13}, \delta_{14}, \delta_{34})$ indicated in the legend, which are different for NH and IH, the number of neutrino and antineutrino events are identical for the two hierarchies. This behavior can be visualized in the right panel of the convoluted bi-events plot shown in figure 1, where the two choices of parameters correspond to the same point (indicated by a star). In this particular case, the distinction between the two mass hierarchies relies solely upon the difference in the shape of the energy spectrum.

panel corresponding to 400 ν_e and 150 $\bar{\nu}_e$ events for both NH and IH is a representative degenerate case, which we intend to discuss in more detail in the following subsection.

4.2 Role of the energy spectrum

The DUNE experiment employs a wide-band energy spectrum, whose shape brings additional information to that given by the total number of events. Therefore, even when there is a complete degeneracy at the level of the total number of events, it is possible to distinguish the two hierarchies at some confidence level. Figure 2 serves to illustrate this point. It represents the expected signal event spectrum of DUNE for the ν_e (left panel) and $\bar{\nu}_e$ (right panel) appearance channels as a function of the reconstructed neutrino energy. The red (blue) histogram corresponds to the case of NH (IH). All the spectra are obtained for $\theta_{34} = 30^\circ$. For the values of the three CP-phases $(\delta_{13}, \delta_{14}, \delta_{34})$ indicated in the legend, which are different for the two hierarchies, the number of neutrino and antineutrino events are identical for the two hierarchies. This fact can be visualized in the right panel of the bi-events plot shown in figure 1, where the two choices of parameters correspond to the same point (indicated by a star). In this particular case, the distinction between the two mass hierarchies relies solely upon the difference in the shape of the energy spectrum, which, as one can appreciate in figure 2, is sizable. Therefore, we expect a good discrimination

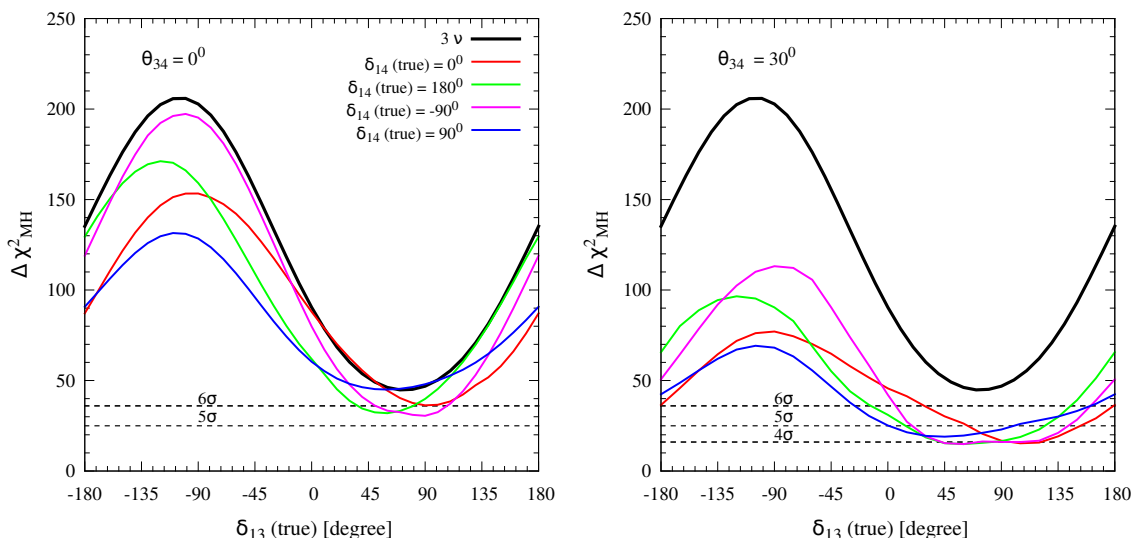


Figure 3. Discovery potential for excluding the wrong hierarchy (IH) as a function of true δ_{13} . In both panels, we have fixed true and test $\theta_{14} = \theta_{24} = 9^\circ$. The left (right) panel refers to true and test $\theta_{34} = 0$ (30°). In each panel, we give the results for the 3-flavor case (black line), and for the 3+1 scheme for four different values of true δ_{14} . In both the panels, we marginalize over test δ_{14} for the 3+1 scheme. On top of this, in the right panel, we also marginalize over true and test choices of the CP-phase δ_{34} over its full allowed range.

potential also for those points which are completely degenerate at the event level. This will be confirmed by the numerical simulation presented in the following, where we find that the pure-shape information is able to guarantee a minimal 4σ level separation between the two mass hierarchies.

4.3 Numerical results

In our numerical analysis we calculate the DUNE discovery potential of the neutrino mass hierarchy. This is defined as the confidence level at which one can exclude the false (or wrong) test hierarchy given a data set generated with the true hierarchy. We have taken the best fit values of all the parameters as given in table 1. In the 3-flavor scheme, we have marginalized over δ_{13} and θ_{23} within their full 3σ range. In the 3+1 scheme, we have also marginalized over the CP-phase δ_{14} (and δ_{34} if $\theta_{34} \neq 0$). In figure 3, we show the discovery potential of excluding the wrong hierarchy as a function of the true value of δ_{13} considering NH as the true hierarchy choice. In each panel, we give the results for the 3-flavor case with the help of thick black curve. In both the panels, for the 3+1 scheme (colored curves), we have taken $\theta_{14} = \theta_{24} = 9^\circ$ while generating the data and also in the fit. In the left panel, we consider $\theta_{34} = 0$ both in data and also in fit, and give the results for four different values of the true δ_{14} (-90° , 90° , 0° , and 180°) while marginalizing over test δ_{14} in its entire range of $[-\pi, \pi]$ in the fit. In the right panel, we show the same considering the true and test $\theta_{34} = 30^\circ$, and therefore, we marginalize over both test δ_{14} and test δ_{34} in their entire ranges of $[-\pi, \pi]$ in the fit. In the right panel, we also marginalize

over true choices of unknown δ_{34} in its full range of $[-\pi, \pi]$ in the data. In the left panel (corresponding to $\theta_{34} = 0$), we observe that the qualitative behavior of the 3+1 curves are similar to the 3-flavor case. In particular, there is a maximum around $\delta_{13} \sim -90^\circ$, and a minimum around $\delta_{13} \sim 90^\circ$. The opposite is true for the IH (not shown). It is evident that in general, there is a deterioration of the discovery potential for all values of the new CP-phase δ_{14} . However, even in the region around the minimum, the sensitivity never drops below 5σ confidence level. In the right panel (corresponding to $\theta_{34} = 30^\circ$), the situation is qualitatively similar, but the sensitivity deteriorates more¹⁰ compared to the left panel. In particular, in the range $\delta_{13} \in [45^\circ, 135^\circ]$, the sensitivity can drop down to 4σ confidence level. This range corresponds to the region of the space spanned by the three CP-phases, where there is basically a complete degeneracy at the level of the total number of events (in both neutrino and antineutrino channels), and the distinction between NH and IH is totally entrusted to the energy spectrum. A concrete example of this kind has been provided in the previous subsection. To this regard, it is important to underline the fundamental difference between the experiments (like DUNE) that make use of an on-axis broad-band neutrino beam, and those using an off-axis configuration (T2K and NO ν A). In this last case, there is basically no spectral information and, as a consequence, there are regions of the parameters space where the MH discovery potential is almost zero (see for example figure 14 in [18]). In a nutshell, in the off-axis configuration, one has basically only the events counting at disposal, while in the on-axis case, there is the extra information coming from the spectral shape. Needless to say, the precondition to take advantage of this additional information is a good understanding of all the ingredients that enter the calculation of the event spectrum, and a refined treatment of the related systematic uncertainties.

5 CP-violation searches in the 3+1 scheme

In this section, we explore the impact of sterile neutrinos in the CPV searches of DUNE. In the 3+1 scheme, there are three CP-phases, all of which can contribute to CPV. We first discuss the discovery potential of the CPV induced by the standard 3-flavor CP-phase $\delta_{13} = \delta$. We will show that, in general, it tends to deteriorate in the 3+1 scheme with respect to the 3-flavor case. Then, we treat the sensitivity to the CPV induced by the other two CP-phases δ_{14} and δ_{34} . Finally, we assess the capability of reconstructing the two phases δ_{13} and δ_{14} .

5.1 CP-violation discovery potential

The discovery potential of CPV induced by a given true δ_{13} is defined as the confidence level at which one can reject the test hypothesis of no CPV i.e. the cases test $\delta_{13} = 0$ and test $\delta_{13} = \pi$ in the fit from that given true δ_{13} . In figure 4, we report the discovery potential of CPV induced by δ_{13} . We show it as a function of the true value of δ_{13} . The left (right) panel refers to true NH (IH). As far as the standard oscillation parameters are concerned, we marginalize over test $\sin^2 \theta_{23}$ in the range 0.34 to 0.68, and over both the

¹⁰We have checked that for the case $\theta_{34} = 9^\circ$, the results are intermediate between those found in the two cases $\theta_{34} = 0$ and $\theta_{34} = 30^\circ$ shown in figure 3. In particular, the minimal sensitivity is approximately 5σ .

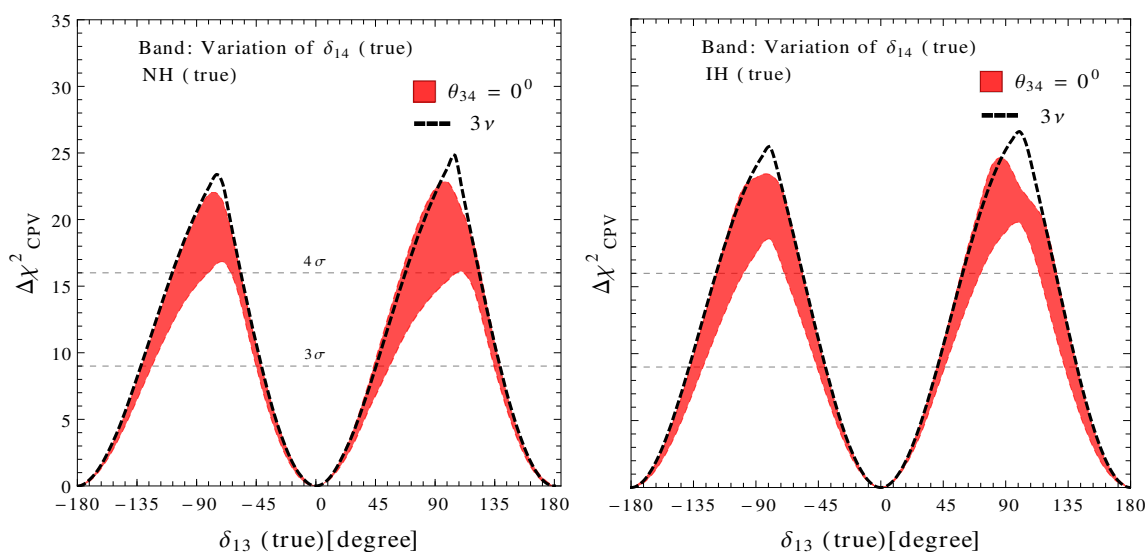


Figure 4. DUNE discovery potential of the CPV induced by δ_{13} . The left (right) panel refers to true NH (IH). In both panels, the black dashed curve corresponds to the 3-flavor case. In 3+1 scenario, we fix the true and test values of $\theta_{14} = \theta_{24} = 9^0$, and we take the true and test θ_{34} to be 0^0 in both the panels. In both the panels, the red bands are obtained in the 3+1 scheme by varying the unknown true δ_{14} in its entire range of $[-\pi, \pi]$ in the data while marginalizing over test δ_{14} in the same range. Both in 3ν and 3+1 schemes, we marginalize over test θ_{23} and over both the choices of test hierarchy.

choices of hierarchy in the fit for both 3ν and 3+1 cases. In both the panels, the black dashed curves correspond to the 3-flavor case. In 3+1 scenario, we fix the true and test values of θ_{14} and θ_{24} to be 9^0 , and we take the true and test θ_{34} to be 0^0 in both the panels, and therefore, δ_{34} becomes irrelevant. In both the panels, the red bands are obtained in the 3+1 scheme by varying the unknown true δ_{14} in its entire range of $[-\pi, \pi]$ in the data while marginalizing over test δ_{14} in the same range. Figure 4 shows that the discovery potential can be deteriorated in the 3+1 scheme as compared to the 3-flavor framework. In particular, around $\delta_{13} \sim \pm 90^0$, where the discovery potential attains the maximal value, the discovery potential can decrease from $\sim 5\sigma$ C.L. (3-flavor case) to $\sim 4\sigma$ C.L. (3+1 case).

In the 3+1 scheme, one expects CPV to come also from the two new phases δ_{14} and δ_{34} . In the second and third panels of figure 5, we display the discovery potential of the CPV induced by such two phases. In the first panel, for the sake of comparison, we report the CPV discovery potential induced by the standard CP-phase δ_{13} so that one can have a global view of the sensitivities. The thinner (magenta) bands correspond to the case in which all the three new mixing angles have the identical true and test values $\theta_{14} = \theta_{24} = \theta_{34} = 9^0$. The thicker (green) bands correspond to the case in which true and test $\theta_{14} = \theta_{24} = 9^0$, and true and test $\theta_{34} = 30^0$. In each panel, the bands have been obtained by varying the true values of the two undisplayed CP-phases in their allowed ranges of $[-\pi, \pi]$ in the data while marginalizing over their test values in the same range in the fit. From the comparison of the three panels, we can see that if all the three mixing

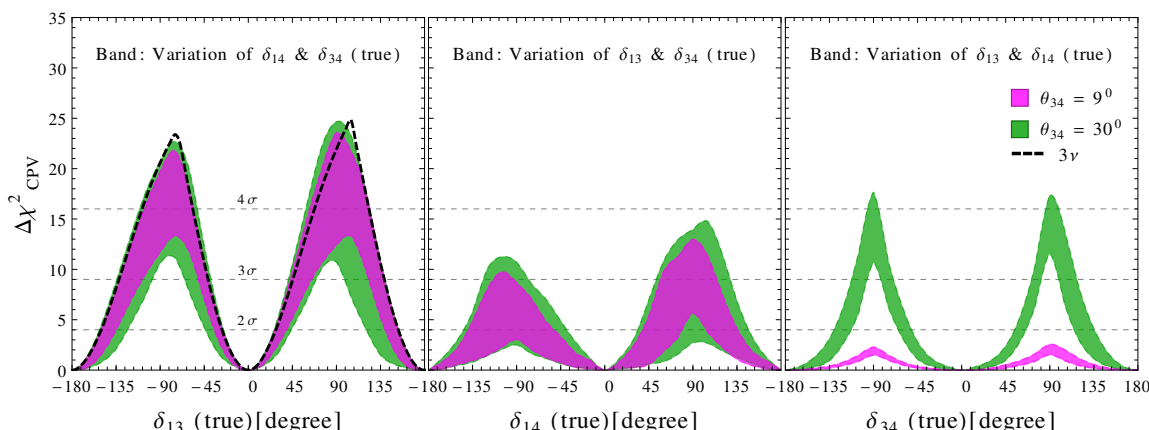


Figure 5. The bands displayed in the left, middle and right panels represent the discovery potential of the CPV induced, respectively, by δ_{13} , δ_{14} and δ_{34} in the 3+1 scheme. The thinner (magenta) bands correspond to the case in which all the three new mixing angles have the identical true and test value $\theta_{14} = \theta_{24} = \theta_{34} = 9^\circ$. The thicker (green) bands correspond to the case in which true and test $\theta_{14} = \theta_{24} = 9^\circ$, and true and test $\theta_{34} = 30^\circ$. In each panel, the bands have been obtained by varying the true values of the two undisplayed CP-phases in their allowed ranges of $[-\pi, \pi]$ in the data while marginalizing over their test values in the same range in the fit. The left panel also reports the 3-flavor curve (black dashed line) for the sake of comparison. In all cases, we marginalize over hierarchy with NH as true choice.

angles have the same value $\theta_{14} = \theta_{24} = \theta_{34} = 9^\circ$ (see the magenta bands), there is a clear hierarchy in the sensitivity to the three CP-phases. The standard phase δ_{13} comes first, δ_{14} comes next, and δ_{34} is the last one, inducing a negligible amount of CPV. In particular, we see that, in the less optimistic cases, corresponding to the lower border of the bands, only the standard CP-phase δ_{13} can give rise to a signal stronger than 3σ for an appreciable fraction of the true values of the phase. This fraction decreases if θ_{34} increases (compare the red band in the left panel of figure 4 with the two bands in the left panel of figure 5). In table 2, for completeness, we report such a fraction for the three values of $\theta_{34} = 0^\circ, 9^\circ$, and 30° as well as for the 3-flavor case. In the same table, we also report as a benchmark the “guaranteed” discovery potential for the particular value $\delta_{13} = -90^\circ$. Concerning the second CP-phase δ_{14} (see the middle panel), the discovery potential spans over a wide band. In favorable cases, one may observe a signal above the 3σ level. However, the lower border of the band is always below the $\sim 2\sigma$ confidence level. This implies that there is not a guaranteed discovery potential at the 3σ confidence level for such a phase. Finally, let us come to the third CP-phase δ_{34} , shown in the right panel. We see that if the mixing angle θ_{34} is very big, the sensitivity can be appreciable. Also, we note that the shape of the band is rather different from that obtained for the other two CP-phases. This different behavior can be understood by observing that in this case, the $\nu_\mu \rightarrow \nu_\mu$ disappearance channel also contributes to the sensitivity. In fact, it is well known that the ν_μ survival probability has a pronounced sensitivity to the NSI-like coupling $\varepsilon_{\mu\tau}$. From the expression of the Hamiltonian in eq. (2.20), one can see that $\varepsilon_{\mu\tau} = rs_{24}\tilde{s}_{34}^*$, hence a sensitivity to the

	θ_{34}	$N\sigma_{\min} [\delta_{13}(\text{true}) = -90^0]$	CPV coverage (3σ)
3ν		4.5	50.0%
$3+1$	0^0	3.9	43.2%
	9^0	3.4	32.0%
	30^0	3.3	16.0%

Table 2. Discovery potential and coverage for the CPV induced by δ_{13} for four benchmark models in the NH case. The first column reports the scheme under consideration. The second column reports the value of θ_{34} (not relevant for the 3ν scheme). The third column reports the discovery potential (in units of standard deviations) for the particular value $\delta_{13} = -90^0$. The fourth column reports the coverage at the 3σ level. Note that in the $3+1$ scheme, the figures reported in the third (fourth) columns represent the minimal “guaranteed” discovery potential (coverage) as derivable from the lower border of the corresponding band in the left panel of figures 4 and 5.

ν_μ survival probability to the CP-phase δ_{34} is expected.¹¹ In order to make this point more clear, in figure 6 we display the partial contributions to the CPV induced by δ_{34} deriving from the $\nu_\mu \rightarrow \nu_e$ channel, the $\nu_\mu \rightarrow \nu_\mu$ channel and from their combination. In this plot we have fixed the test value of θ_{23} at its true (maximal) value because the $\nu_\mu \rightarrow \nu_e$ channel, when taken alone, has a limited sensitivity to this parameter. Finally, we remark that the $\nu_\mu \rightarrow \nu_\mu$ channel has almost no role in the sensitivity to the other two CP-phases δ_{13} and δ_{14} , as we have explicitly verified numerically.

5.2 Reconstruction of the CP-phases

In the previous subsection, we have focused our attention on the discovery potential of the CPV arising from the three CP-phases involved in the $3+1$ scheme. However, we deem it important to pursue the exploration of the CP-phases independently of the amount of CPV (if any) that they may generate. In principle, any value of the CP-phases is plausible, including the CP-conserving cases. According to this point of view, one should try to answer the following question: what is the capability of reconstructing the true values of the CP-phases. In the following, we address this issue, confining our study to the two CP-phases δ_{13} and δ_{14} , to which one expects to have a more pronounced sensitivity.

In figure 7, we have performed this exercise under the assumption that true and test values of $\theta_{34} = 0$, and therefore, the third CP-phase δ_{34} becomes irrelevant. In each panel, we show the regions reconstructed around the representative true values of δ_{13} and δ_{14} . In all cases, we have taken the NH as the true hierarchy in the data, and then marginalized over both NH and IH in theory. However, we find that the marginalization procedure never selects the wrong hierarchy. Hence, there is no degeneracy between mass hierarchy and the CP-phases. Similar results (not shown) are obtained for the IH case. The two

¹¹It should be noted that the ν_μ survival probability depends only on the real part of the new dynamical NSI-like coupling $\text{Re}(\varepsilon_{\mu\tau}) = \text{Re}(rs_{24}\tilde{s}_{34}^*) = rs_{24}s_{34} \cos \delta_{34}$. This implies that the sensitivity to δ_{34} is attained only via terms proportional to $\cos \delta_{34}$. This feature is reflected in the particular shape of the blue band in figure 6, which is symmetrical under a reflection around $\delta_{34} = 0^0$, i.e., under the transformation $\delta_{34} \rightarrow -\delta_{34}$. It is worth noticing that while the $\cos \delta_{34}$ term does not give rise to manifest CPV, its measurement allows one to establish the existence of CPV indirectly.

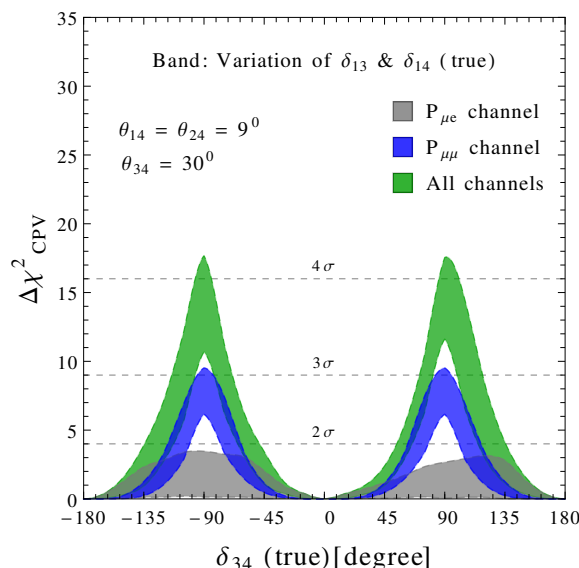


Figure 6. Partial contributions to the sensitivity to the CPV induced by the phase δ_{34} deriving from different channels and from their combination. The gray band is the contribution from ν_e and $\bar{\nu}_e$ appearance, the blue band refers to the ν_μ and $\bar{\nu}_\mu$ disappearance, and the green band is the global sensitivity obtained including all channels. The three new mixing angles have been fixed to $\theta_{14} = \theta_{24} = 9^\circ$ and $\theta_{34} = 30^\circ$. The mixing angle θ_{23} has been fixed to be maximal (both true and test value). We marginalize over hierarchy with NH as true choice.

upper panels refer to two representative CP-conserving scenarios $[0, 0]$ and $[\pi, \pi]$. The third and fourth panels refer to two representative CP-violating cases $[-\pi/2, -\pi/2]$ and $[\pi/2, \pi/2]$. The two confidence levels correspond to 2σ and 3σ (1 d.o.f.). We see that in all cases we obtain a unique reconstructed region at the 3σ level.¹² The typical 1σ level uncertainty on the reconstructed CP-phases is approximately 20° (30°) for δ_{13} (δ_{14}). The regions in figure 7 should be compared with the analogous ones obtained with the combination of the prospective data of T2K and NO ν A (see figure 13 in [18]). From such a comparison, one can see that DUNE is much more effective in the reconstruction of the CP-phases. In fact, in the combination of T2K and NO ν A, a good reconstruction is possible only at the 1σ confidence level, and in favorable cases, at the 2σ level. At higher confidence levels, the reconstruction capability basically disappears. In DUNE, the situation is much improved. This is imputable both to the higher statistics and to the spectral shape information attainable from the wide-band neutrino flux.

We close our discussion on the CP-phases by showing the impact of θ_{34} and of the ignorance of the related CP-phase δ_{34} on the reconstruction of the two CP-phases δ_{13} and δ_{14} . Figure 8 is analogous to figure 7, but now, we assume $\theta_{34} = 30^\circ$ both in data and in theory. In this case, the transition probability depends also on the third CP-phase δ_{34} . Since it is unknown, one has to marginalize over the true and test values of this CP-phase while reconstructing the other two phases. As evident from all panels of figure 8, the quality of the reconstruction deteriorates. In particular, the uncertainty on δ_{14} increases roughly

¹²Note that this is true also in the second panel, because the four corners of the square form a connected region due to the cyclic nature of the two CP-phases.

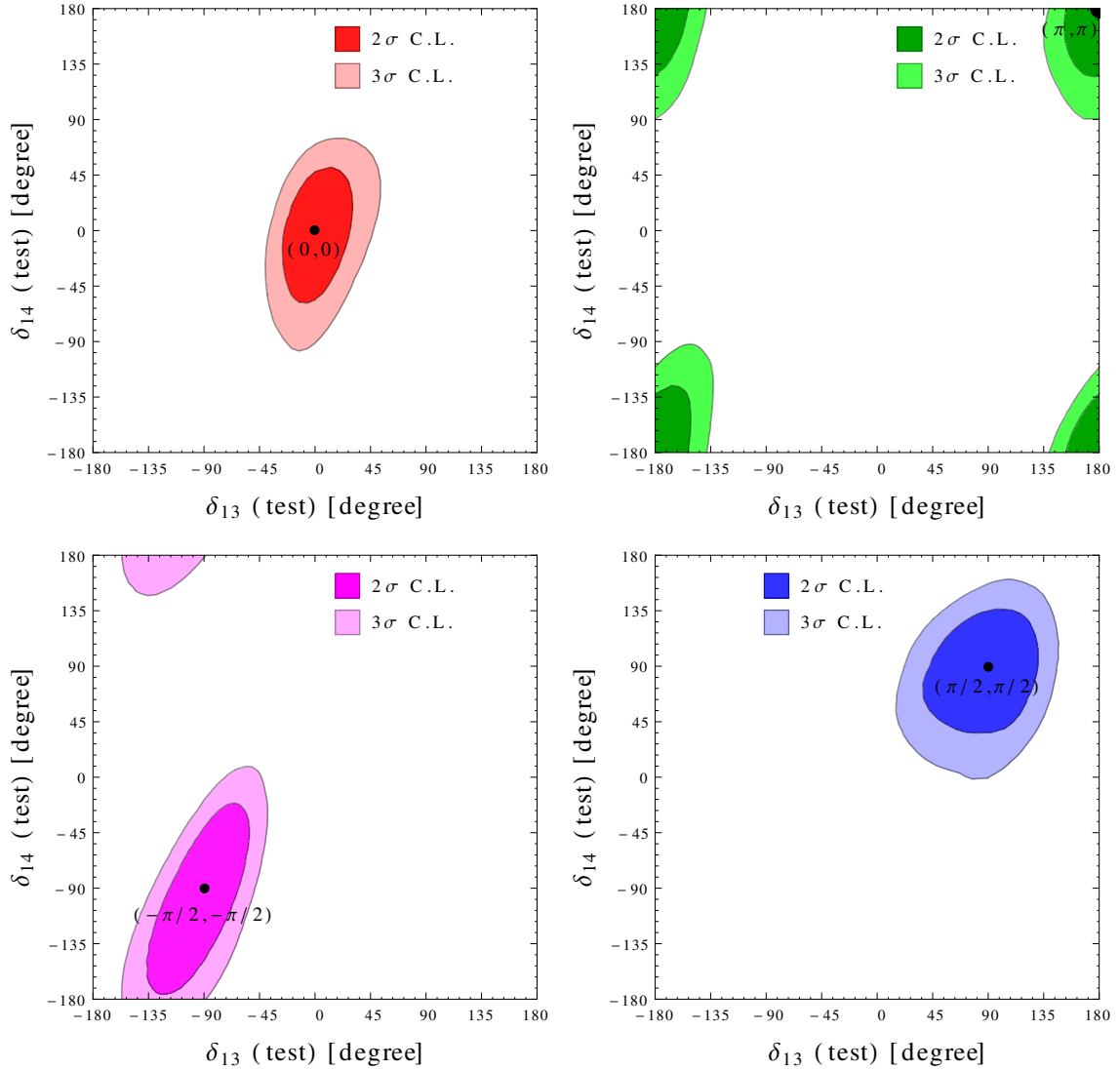


Figure 7. Reconstructed regions for the two CP-phases δ_{13} and δ_{14} for the four choices of their true values indicated in each panel. The NH is taken as the true hierarchy, while we have marginalized over the two possible hierarchies in the test model. The contours refer to 2σ and 3σ levels. We have fixed the values $\theta_{34}(\text{true}) = 0^0$.

by two times (from $\sim 30^0$ to $\sim 60^0$), while that on δ_{13} remains basically unchanged (still around $\sim 25^0$). Hence, the reconstruction of the standard CP-phase δ_{13} is more robust than that of new CP-phase δ_{14} with respect to the perturbations induced by a large value of the mixing angle θ_{34} . This behavior can be traced to the fact that, differently from δ_{13} , the two new CP-phases δ_{14} and δ_{34} both enter at the dynamical level [see eqs. (2.20)–(2.21)], and in particular, in the NSI-like matrix element $\varepsilon_{e\tau} \propto \tilde{s}_{14}\tilde{s}_{34}^*$. Therefore, one may expect a certain degree of degeneracy among the two new CP-phases, which in the marginalization process over the undisplayed CP-phase δ_{34} , translates into a deterioration in the reconstruction of δ_{14} .

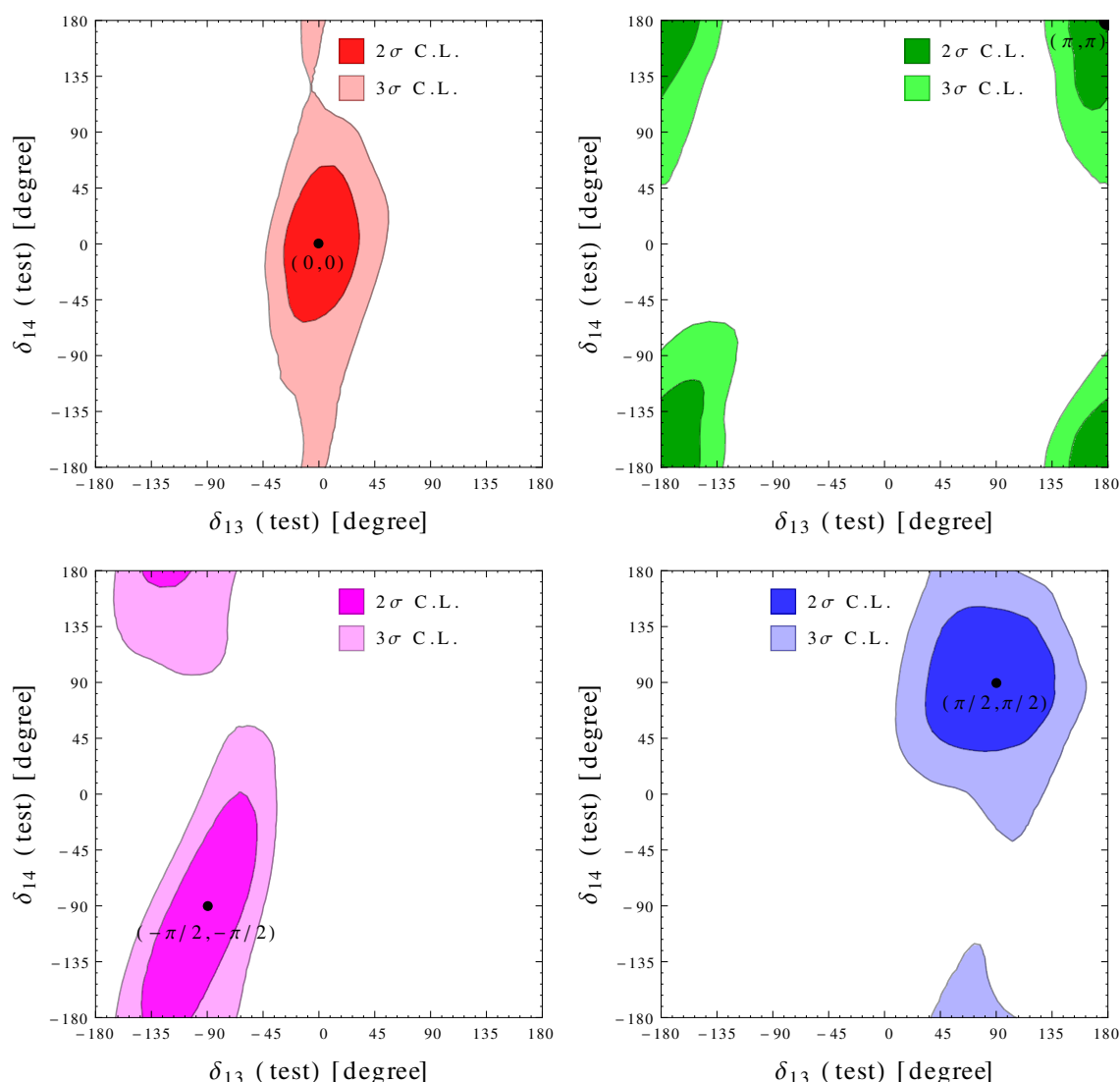


Figure 8. Reconstructed regions for the two CP-phases δ_{13} and δ_{14} for the four choices of their true values indicated in each panel. The NH is taken as the true hierarchy, while we have marginalized over the two possible hierarchies in the test model. The contours refer to 2σ and 3σ confidence levels. We have fixed θ_{34} (true) = 30° , and have marginalized over δ_{34} (both true and test values) over its range of variability.

6 Conclusions and outlook

We have investigated the impact of one light eV scale sterile neutrino on the prospective data expected to be collected at the planned long-baseline experiment DUNE. We have found that the discovery potential of the neutrino mass hierarchy (MH), remains above 5σ confidence level if all the three new mixing angles are relatively small ($\theta_{14} = \theta_{24} = \theta_{34} = 9^\circ$). In contrast, if the third mixing angle θ_{34} is taken at its upper limit ($\theta_{34} = 30^\circ$), the MH sensitivity can drop to 4σ confidence level. Our analysis has clearly shown that

the spectral information attainable from the wide-band spectrum employed by DUNE is crucial to preserve a good sensitivity to the MH also in the 3+1 scheme. We have also assessed the sensitivity to the CPV induced both by the standard CP-phase $\delta_{13} \equiv \delta$, and by the new CP-phases (δ_{14} and δ_{34} in our parametrization). We have found that the performance of DUNE in claiming the discovery of CPV induced by δ_{13} gets deteriorated as compared to the 3-flavor case. In particular, the maximal sensitivity (reached around $\delta_{13} \sim \pm 90^\circ$) decreases from 5σ to 4σ confidence level if all the three new mixing angles are small ($\theta_{14} = \theta_{24} = \theta_{34} = 9^\circ$), and can drop almost to 3σ confidence level if $\theta_{34} = 30^\circ$. The sensitivity to the CPV induced by the new CP-phase δ_{14} can reach 3σ C.L. for an appreciable fraction of its true values, but never reaches 4σ confidence level. The sensitivity to the third CP-phase δ_{34} , which arises exclusively through matter effects, is appreciable only if θ_{34} is large. Interestingly, we have found that the sensitivity to δ_{34} stems from both the ν_e appearance and ν_μ disappearance channels. We have finally investigated the capability of DUNE in reconstructing the true values of the two CP-phases δ_{13} and δ_{14} . The typical 1σ level uncertainty on the reconstructed CP-phase δ_{13} (δ_{14}) is approximately 20° (30°) provided $\theta_{34} = 0$. But, in case of large θ_{34} , the reconstruction of δ_{14} (but not that of δ_{13}) becomes poor. So, finally, we can conclude that the results presented in this paper clearly demonstrates that in the presence of a light eV-scale sterile neutrino, the proposed LBL experiments such as DUNE would be quite sensitive to the new CP-phases associated to the sterile state, and therefore, would play a complementary role to the SBL experiments.

Acknowledgments

S.K.A. is supported by the DST/INSPIRE Research Grant [IFA-PH-12], Department of Science & Technology, India. A.P. is supported by the Grant “Future In Research” *Beyond three neutrino families*, contract no. YVI3ST4, of Regione Puglia, Italy.

Open Access. This article is distributed under the terms of the Creative Commons Attribution License ([CC-BY 4.0](https://creativecommons.org/licenses/by/4.0/)), which permits any use, distribution and reproduction in any medium, provided the original author(s) and source are credited.

References

- [1] S. Pascoli and T. Schwetz, *Prospects for neutrino oscillation physics*, *Adv. High Energy Phys.* **2013** (2013) 503401.
- [2] S.K. Agarwalla, S. Prakash and S. Uma Sankar, *Exploring the three flavor effects with future superbeams using liquid argon detectors*, *JHEP* **03** (2014) 087 [[arXiv:1304.3251](https://arxiv.org/abs/1304.3251)] [[INSPIRE](#)].
- [3] S.K. Agarwalla, *Physics Potential of Long-Baseline Experiments*, *Adv. High Energy Phys.* **2014** (2014) 457803 [[arXiv:1401.4705](https://arxiv.org/abs/1401.4705)] [[INSPIRE](#)].
- [4] G.J. Feldman, J. Hartnell and T. Kobayashi, *Long-baseline neutrino oscillation experiments*, *Adv. High Energy Phys.* **2013** (2013) 475749 [[arXiv:1210.1778](https://arxiv.org/abs/1210.1778)] [[INSPIRE](#)].
- [5] L. Stanco, *A View of Neutrino Studies with the Next Generation Facilities*, *Rev. Phys.* **1** (2016) 90 [[arXiv:1511.09409](https://arxiv.org/abs/1511.09409)] [[INSPIRE](#)].

- [6] N. Klop and A. Palazzo, *Imprints of CP-violation induced by sterile neutrinos in T2K data*, *Phys. Rev. D* **91** (2015) 073017 [[arXiv:1412.7524](#)] [[INSPIRE](#)].
- [7] K.N. Abazajian et al., *Light Sterile Neutrinos: A White Paper*, [arXiv:1204.5379](#) [[INSPIRE](#)].
- [8] A. Palazzo, *Phenomenology of light sterile neutrinos: a brief review*, *Mod. Phys. Lett. A* **28** (2013) 1330004 [[arXiv:1302.1102](#)] [[INSPIRE](#)].
- [9] S. Gariazzo, C. Giunti, M. Laveder, Y.F. Li and E.M. Zavanin, *Light sterile neutrinos*, *J. Phys. G* **43** (2016) 033001 [[arXiv:1507.08204](#)] [[INSPIRE](#)].
- [10] T. Lasserre, *Light Sterile Neutrinos in Particle Physics: Experimental Status*, *Phys. Dark Univ.* **4** (2014) 81 [[arXiv:1404.7352](#)] [[INSPIRE](#)].
- [11] C. Giunti, M. Laveder, Y.F. Li and H.W. Long, *Pragmatic View of Short-Baseline Neutrino Oscillations*, *Phys. Rev. D* **88** (2013) 073008 [[arXiv:1308.5288](#)] [[INSPIRE](#)].
- [12] J. Kopp, P.A.N. Machado, M. Maltoni and T. Schwetz, *Sterile Neutrino Oscillations: The Global Picture*, *JHEP* **05** (2013) 050 [[arXiv:1303.3011](#)] [[INSPIRE](#)].
- [13] A. Palazzo, *3-flavor and 4-flavor implications of the latest T2K and NOvA electron (anti-)neutrino appearance results*, *Phys. Lett. B* **757** (2016) 142 [[arXiv:1509.03148](#)] [[INSPIRE](#)].
- [14] A. Palazzo, *Consistent analysis of the $\nu_\mu \rightarrow \nu_e$ sterile neutrinos searches of ICARUS and OPERA*, *Phys. Rev. D* **91** (2015) 091301 [[arXiv:1503.03966](#)] [[INSPIRE](#)].
- [15] M. Antonello et al., *Experimental search for the “LSND anomaly” with the ICARUS detector in the CNGS neutrino beam*, *Eur. Phys. J. C* **73** (2013) 2345 [[arXiv:1209.0122](#)] [[INSPIRE](#)].
- [16] M. Antonello et al., *Some conclusive considerations on the comparison of the ICARUS $\nu_\mu \rightarrow \nu_e$ oscillation search with the MiniBooNE low-energy event excess*, [arXiv:1502.04833](#) [[INSPIRE](#)].
- [17] OPERA collaboration, N. Agafonova et al., *Search for $\nu_\mu \rightarrow \nu_e$ oscillations with the OPERA experiment in the CNGS beam*, *JHEP* **07** (2013) 004 [Addendum *ibid.* **07** (2013) 085] [[arXiv:1303.3953](#)] [[INSPIRE](#)].
- [18] S.K. Agarwalla, S.S. Chatterjee, A. Dasgupta and A. Palazzo, *Discovery Potential of T2K and NOvA in the Presence of a Light Sterile Neutrino*, *JHEP* **02** (2016) 111 [[arXiv:1601.05995](#)] [[INSPIRE](#)].
- [19] S.K. Agarwalla, T. Li and A. Rubbia, *An incremental approach to unravel the neutrino mass hierarchy and CP-violation with a long-baseline Superbeam for large θ_{13}* , *JHEP* **05** (2012) 154 [[arXiv:1109.6526](#)] [[INSPIRE](#)].
- [20] LAGUNA-LBNO collaboration, S.K. Agarwalla et al., *The mass-hierarchy and CP-violation discovery reach of the LBNO long-baseline neutrino experiment*, *JHEP* **05** (2014) 094 [[arXiv:1312.6520](#)] [[INSPIRE](#)].
- [21] HYPER-KAMIOKANDE WORKING GROUP collaboration, K. Abe et al., *A Long Baseline Neutrino Oscillation Experiment Using J-PARC Neutrino Beam and Hyper-Kamiokande*, [arXiv:1412.4673](#) [[INSPIRE](#)].
- [22] HYPER-KAMIOKANDE PROTO-COLLABORATION collaboration, K. Abe et al., *Physics potential of a long-baseline neutrino oscillation experiment using a J-PARC neutrino beam and Hyper-Kamiokande*, *PTEP* **2015** (2015) 053C02 [[arXiv:1502.05199](#)] [[INSPIRE](#)].

- [23] D. Hollander and I. Mocioiu, *Minimal 3+2 sterile neutrino model at LBNE*, *Phys. Rev. D* **91** (2015) 013002 [[arXiv:1408.1749](#)] [[INSPIRE](#)].
- [24] J.M. Berryman, A. de Gouvêa, K.J. Kelly and A. Kobach, *Sterile neutrino at the Deep Underground Neutrino Experiment*, *Phys. Rev. D* **92** (2015) 073012 [[arXiv:1507.03986](#)] [[INSPIRE](#)].
- [25] R. Gandhi, B. Kayser, M. Masud and S. Prakash, *The impact of sterile neutrinos on CP measurements at long baselines*, *JHEP* **11** (2015) 039 [[arXiv:1508.06275](#)] [[INSPIRE](#)].
- [26] A. Donini and D. Meloni, *The 2+2 and 3+1 four family neutrino mixing at the neutrino factory*, *Eur. Phys. J. C* **22** (2001) 179 [[hep-ph/0105089](#)] [[INSPIRE](#)].
- [27] A. Donini, M. Lusignoli and D. Meloni, *Telling three neutrinos from four neutrinos at the neutrino factory*, *Nucl. Phys. B* **624** (2002) 405 [[hep-ph/0107231](#)] [[INSPIRE](#)].
- [28] A. Donini, M. Maltoni, D. Meloni, P. Migliozi and F. Terranova, *3+1 sterile neutrinos at the CNGS*, *JHEP* **12** (2007) 013 [[arXiv:0704.0388](#)] [[INSPIRE](#)].
- [29] A. Dighe and S. Ray, *Signatures of heavy sterile neutrinos at long baseline experiments*, *Phys. Rev. D* **76** (2007) 113001 [[arXiv:0709.0383](#)] [[INSPIRE](#)].
- [30] A. Donini, K.-i. Fuki, J. Lopez-Pavon, D. Meloni and O. Yasuda, *The discovery channel at the Neutrino Factory: $\nu_\mu \rightarrow \nu_\tau$ pointing to sterile neutrinos*, *JHEP* **08** (2009) 041 [[arXiv:0812.3703](#)] [[INSPIRE](#)].
- [31] O. Yasuda, *Sensitivity to sterile neutrino mixings and the discovery channel at a neutrino factory*, [arXiv:1004.2388](#) [[INSPIRE](#)].
- [32] D. Meloni, J. Tang and W. Winter, *Sterile neutrinos beyond LSND at the Neutrino Factory*, *Phys. Rev. D* **82** (2010) 093008 [[arXiv:1007.2419](#)] [[INSPIRE](#)].
- [33] B. Bhattacharya, A.M. Thalapillil and C.E.M. Wagner, *Implications of sterile neutrinos for medium/long-baseline neutrino experiments and the determination of θ_{13}* , *Phys. Rev. D* **85** (2012) 073004 [[arXiv:1111.4225](#)] [[INSPIRE](#)].
- [34] A. Donini, P. Hernández, J. Lopez-Pavon, M. Maltoni and T. Schwetz, *The minimal 3+2 neutrino model versus oscillation anomalies*, *JHEP* **07** (2012) 161 [[arXiv:1205.5230](#)] [[INSPIRE](#)].
- [35] F. Capozzi, E. Lisi, A. Marrone, D. Montanino and A. Palazzo, *Neutrino masses and mixings: Status of known and unknown 3ν parameters*, *Nucl. Phys. B* **908** (2016) 218 [[arXiv:1601.07777](#)] [[INSPIRE](#)].
- [36] D.V. Forero, M. Tortola and J.W.F. Valle, *Neutrino oscillations refitted*, *Phys. Rev. D* **90** (2014) 093006 [[arXiv:1405.7540](#)] [[INSPIRE](#)].
- [37] M.C. Gonzalez-Garcia, M. Maltoni and T. Schwetz, *Updated fit to three neutrino mixing: status of leptonic CP-violation*, *JHEP* **11** (2014) 052 [[arXiv:1409.5439](#)] [[INSPIRE](#)].
- [38] A. Palazzo, *Testing the very-short-baseline neutrino anomalies at the solar sector*, *Phys. Rev. D* **83** (2011) 113013 [[arXiv:1105.1705](#)] [[INSPIRE](#)].
- [39] DUNE collaboration, R. Acciarri et al., *Long-Baseline Neutrino Facility (LBNF) and Deep Underground Neutrino Experiment (DUNE) Conceptual Design Report Volume 1: The LBNF and DUNE Projects*, [arXiv:1601.05471](#) [[INSPIRE](#)].
- [40] DUNE collaboration, R. Acciarri et al., *Long-Baseline Neutrino Facility (LBNF) and Deep Underground Neutrino Experiment (DUNE) Conceptual Design Report Volume 2: The Physics Program for DUNE at LBNF*, [arXiv:1512.06148](#) [[INSPIRE](#)].

- [41] DUNE collaboration, J. Strait et al., *Long-Baseline Neutrino Facility (LBNF) and Deep Underground Neutrino Experiment (DUNE) Conceptual Design Report Volume 3: Long-Baseline Neutrino Facility for DUNE June 24, 2015*, [arXiv:1601.05823](#) [[INSPIRE](#)].
- [42] DUNE collaboration, R. Acciarri et al., *Long-Baseline Neutrino Facility (LBNF) and Deep Underground Neutrino Experiment (DUNE) Conceptual Design Report, Volume 4 The DUNE Detectors at LBNF*, [arXiv:1601.02984](#) [[INSPIRE](#)].
- [43] LBNE collaboration, C. Adams et al., *The Long-Baseline Neutrino Experiment: Exploring Fundamental Symmetries of the Universe*, [arXiv:1307.7335](#) [[INSPIRE](#)].
- [44] ICARUS collaboration, S. Amerio et al., *Design, construction and tests of the ICARUS T600 detector*, *Nucl. Instrum. Meth. A* **527** (2004) 329 [[INSPIRE](#)].
- [45] M. Bishai, private communication (2012).
- [46] P. Huber, M. Lindner and W. Winter, *Simulation of long-baseline neutrino oscillation experiments with GLoBES (General Long Baseline Experiment Simulator)*, *Comput. Phys. Commun.* **167** (2005) 195 [[hep-ph/0407333](#)] [[INSPIRE](#)].
- [47] P. Huber, J. Kopp, M. Lindner, M. Rolinec and W. Winter, *New features in the simulation of neutrino oscillation experiments with GLoBES 3.0: General Long Baseline Experiment Simulator*, *Comput. Phys. Commun.* **177** (2007) 432 [[hep-ph/0701187](#)] [[INSPIRE](#)].
- [48] M.D. Messier, *Evidence for neutrino mass from observations of atmospheric neutrinos with Super-Kamiokande*, Ph.D. Thesis, advisor: J.L. Stone (1999) [[INSPIRE](#)].
- [49] E.A. Paschos and J.Y. Yu, *Neutrino interactions in oscillation experiments*, *Phys. Rev. D* **65** (2002) 033002 [[hep-ph/0107261](#)] [[INSPIRE](#)].
- [50] G. Zeller, private communication (2012).
- [51] R. Petti and G. Zeller, *Nuclear Effects in Water vs. Argon*, Tech. Rep. LBNE docdb No. 740.
- [52] A.M. Dziewonski and D.L. Anderson, *Preliminary reference earth model*, *Phys. Earth Planet In.* **25** (1981) 297.
- [53] P. Huber, M. Lindner and W. Winter, *Superbeams versus neutrino factories*, *Nucl. Phys. B* **645** (2002) 3 [[hep-ph/0204352](#)] [[INSPIRE](#)].
- [54] G.L. Fogli, E. Lisi, A. Marrone, D. Montanino and A. Palazzo, *Getting the most from the statistical analysis of solar neutrino oscillations*, *Phys. Rev. D* **66** (2002) 053010 [[hep-ph/0206162](#)] [[INSPIRE](#)].
- [55] M. Blennow, P. Coloma, P. Huber and T. Schwetz, *Quantifying the sensitivity of oscillation experiments to the neutrino mass ordering*, *JHEP* **03** (2014) 028 [[arXiv:1311.1822](#)] [[INSPIRE](#)].